Numerical solution of the 1-D grey radiation hydrodynamics equations with an entropy-based artificial viscosity

Marc O. Delchini[a], Jim Morel[a], Jean C. Ragusa[a,*]

[a] *Department of Nuclear Engineering, Texas A&M University, College Station, TX 77843, USA*

Abstract

The entropy viscosity method is extended to the 1-D grey radiation-hydrodynamic equations. The method employs a viscous regularization to stabilize the numerical scheme with a viscosity coefficient modulated by the entropy production that is known to peak in shocks. The dissipative terms are consistent with the entropy minimum principle which requires that a new functional form of the entropy residual, suitable for the radiation-hydrodynamic equations, be derived. The equations are discretized with a standard Continuous Galerkin Finite Element Method (CGFEM) and an implicit temporal integrator within the MOOSE multiphysics framework. The method of manufactured solution (MMS) is employed to demonstrate second-order accuracy in both the equilibrium diffusion and streaming limits. Several typical 1-D radiation-hydrodynamic test cases with shocks (from Mach 1.05 to Mach 50) are computed to establish the ability of the technique to capture and resolve shocks.

Keywords: radiation-hydrodynamic, shock, entropy viscosity method, high-order viscous stabilization method.

*Corresponding author

Email addresses: delchmo@tamu.edu (Marc O. Delchini), jim.morel@tamu.edu (Jim Morel), jean.ragusa@tamu.edu (Jean C. Ragusa)

1. Introduction

Solving the radiation hydrodynamic equations is a challenging task for multiple reasons. First, the characteristic time scales between the radiation and hydrodynamics are different by several orders of magnitude which often requires the radiation part to be solved implicitly to ensure stability. Second, as with any wave-dominated problems, high resolution schemes are needed to accurately resolve shocks. Third, achieving high-order accuracy is challenging but some recent developments provided high-order accuracy results both in time and space when discretizing either the Euler equations [1, 2, 3, 4] or the radiation equation independently from each other.

Significant effort has been put into developing Riemann solvers for both the radiation and hydrodynamic equations. Balsara [5] developed a Riemann solver for the radiation-hydrodynamic equations by considering the frozen approximation that decouples the two physics components. However, such an approach may be questionable in the equilibrium diffusion limit. In this case, the coupling terms drive the physics and have to be accounted for. A *generalized Riemann solver* that accounts exactly for the relaxation terms was developed in [5]. Another approach assumes the strong equilibrium diffusion limit in which radiation diffusion is negligible and the radiation simply advects at the material velocity [6]. In this limit, the radiation hydrodynamics equation can be expressed in the form of the Euler equations with a radiation-modified equation of state (REOS) . Any solution technique for the Euler equations may be applied to these equations. Thus, one may develop approximate Riemann solvers for these equations and applied them in a general context.

Edwards and al. [7] proposed a two-stage semi-implicit IMEX scheme to solve the radiation-hydrodynamic equations. Riemann solver along with a flux limiter is used to resolve shocks and other waves. Their results show good agreement with semi-analytical solutions.

In this article we propose to solve the 1-D radiation-hydrodynamics equations by using *the entropy viscosity method*. This technique, developed by Guer-

mond et al. for hyperbolic systems of equations [2, 3], consists in adding appropriate dissipative terms to the governing equations. The viscosity coefficient of these terms is modulated by the local entropy production. These dissipative terms are devised to stabilize the numerical scheme and to remove the non-physical oscillations appearing at the shock locations. Generally speaking, entropy is produced at shocks [8]. Thus, by setting the viscosity coefficient proportional to the entropy production, shocks can be detected and tracked and an adequate amount of viscosity is added locally to stabilize the numerical scheme. The entropy production is computed on the fly, by analyzing the entropy residual. This residual is strongly peaked in shocks and small elsewhere. The entropy viscosity method was shown to achieve high-order accuracy away from the shock regions, was successfully applied to non-linear hyperbolic equations using various discretization methods (finite volume, continuous and discontinuous finite elements, spectral method) and yielded high-order accuracy on non-uniform meshes and complex geometries [3, 9]. Because of the similarity between Euler equations and the radiation hydrodynamic equations, it is conjectured that the entropy viscosity method may be a good candidate for resolving shocks occurring in radiation-hydrodynamic phenomena.

The 1-D grey radiation-hydrodynamic (GRH) equations are recalled in Eq. (1):

$$\begin{cases} \partial_t(\rho) + \partial_x(\rho u) = 0 \\ \partial_t(\rho u) + \partial_x\left(\rho u^2 + P + \frac{\epsilon}{3}\right) = 0 \\ \partial_t(\rho E) + \partial_x\left[u(\rho E + P)\right] = -\frac{u}{3}\partial_x\epsilon - \sigma_a c\left(aT^4 - \epsilon\right) \\ \partial_t\epsilon + \frac{4}{3}\partial_x(u\epsilon) = \frac{u}{3}\partial_x\epsilon + \partial_x\left(\frac{c}{3\sigma_t}\partial_x\epsilon\right) + \sigma_a c\left(aT^4 - \epsilon\right) \end{cases}, \tag{1}$$

where ρ, u, E, ϵ, P and T are the material density, material velocity, material specific total energy, radiation energy density, material pressure and temperature, respectively. The total and absorption cross sections, σ_t and σ_a, are either constant or density- and temperature-dependent. The variables a and c are the Boltzman constant and the speed of light, respectively. Lastly, the symbols ∂_t and ∂_x denote the temporal and spatial partial derivatives, respectively. The

material temperature and pressure are computed with the Ideal Gas equation of state (IGEOS):

$$\begin{cases} P = (\gamma - 1) C_v \rho T \\ e = C_v T \end{cases}, \tag{2}$$

where e is the specific internal energy and is obtained from the expression $e = E - 0.5u^2$. The heat capacity C_v and the heat ratio coefficient γ are assumed constant.

The objective of this paper is to extend the entropy-based viscosity method to the 1-D grey radiation-hydrodynamic equations. The approach followed in this paper is similar to those of [5, 10] in order to make Eq. (1) hyperbolic. Then, an entropy equation is derived and used to obtain the functional forms of the viscous stabilization terms. Definitions for the viscosity coefficients are provided.

This paper is organized as follows. In Section 2, the entropy viscosity method is extended to the grey radiation-hydrodynamic equations; details regarding the derivation of the adequate dissipative terms and definitions for the new viscosity coefficients are provided. Spatial and temporal discretization schemes are discussed in Section 3 along with the solution algorithm employed to solve the discretized equations. Numerical results are presented in Section 4 where the second-order accuracy of the scheme is demonstrated in both the equilibrium diffusion and streaming limits, using the method of manufactured solutions applied to the GRH equations. Then, several numerical test cases, taken from the published literature, are provided; in these simulations, the Mach number varies from 1.05 to 50 [11]. Conclusions are presented in Section 5.

2. The entropy-based viscosity method applied to the 1-D Radiation-Hydrodynamic equations

In this section, we extend the entropy viscosity method [2, 3, 9] to the 1-D radiation-hydrodynamic equations in a staged process. First, the reader is guided through the main steps that lead to the derivation of a viscous regular-

ization, using the entropy minimum principle [12]. Then, an asymptotic study is performed onto the system of equations modified with the viscous regularization, to show that the equilibrium-diffusion limit is recovered [10]. Lastly, a definition for the entropy viscosity coefficient derived along with the viscous regularizations is proposed and based upon the entropy production.

2.1. Derivation of a viscous regularization for the 1-D grey non-equilibrium Radiation-Hydrodynamic equations

We recall that the entropy viscosity method was developed for hyperbolic system of equations. However, the radiation hydrodynamic equations are not strictly hyperbolic but several numerical techniques are based on the study of their hyperbolic parts [5, 10]. Thus, following the same rationale, the system of equations given in Eq. (1) is made hyperbolic by ignoring the relaxation and the diffusion terms in the radiation and material energy equations. These two assumptions yield the following system of equations:

$$\begin{cases} \partial_t(\rho) + \partial_x(\rho u) = 0 \\ \partial_t(\rho u) + \partial_x\left(\rho u^2 + P + \frac{\epsilon}{3}\right) = 0 \\ \partial_t(\rho E) + \partial_x\left[u(\rho E + P)\right] + \frac{u}{3}\partial_x\epsilon = 0 \\ \partial_t\epsilon + \frac{4}{3}\partial_x(u\epsilon) - \frac{u}{3}\partial_x\epsilon = 0 \end{cases} . \tag{3}$$

The jacobian matrix of the hyperbolic terms can be computed to derive the eigenvalues:

$$\lambda_1 = u - c_m,\ \lambda_{2,3} = u \text{ and } \lambda_4 = u + c_m, \tag{4}$$

where c_m is the radiation-modified material speed of sound and is defined as follows:

$$c_m^2 = \underbrace{P_\rho + \frac{P}{\rho^2}P_e}_{c_{Euler}^2} + \frac{4\epsilon}{9\rho} = c_{Euler}^2 + c_{rad}^2 \ . \tag{5}$$

P_x is the standard shorthand notation for $\partial_x P$, c_{Euler}^2 denotes the definition of the speed of sound when considering only the 1-D Euler equations and c_{rad}^2 is the radiation contribution to the sound speed c_m^2. The eigenvalues given

in Eq. (4) are unconditionally real. Because the above system is hyperbolic, we can assume the existence of an entropy function s [13] that depends upon the internal energy e, the density ρ, and the radiation energy density ϵ (three primitive variables). Following some algebra given in Appendix A, an equation satisfied by the entropy s is obtained:

$$\rho \frac{Ds}{Dt} = \rho \left(\partial_t s + u \partial_x s \right) = 0, \tag{6}$$

where $\frac{D\cdot}{Dt}$ denotes the total or material derivative. Eq. (6) is often referred as the entropy residual and is used to prove the entropy minimum principle, $\frac{Ds}{Dt} \geq 0$, [12] when the solution remains smooth.

We propose to modify Eq. (3) by adding dissipative terms to keep the solution smooth when shocks develop. When adding dissipative terms to each equation of Eq. (3) as required in the entropy viscosity method, the entropy residual equation is modified and some additional terms will appear in the right-hand side of Eq. (6). The sign of these extra terms needs to be studied for the entropy minimum principle to hold. As such, the entropy minimum principle is invoked to guide in the derivation of appropriate expressions for each of the dissipative terms. Obtaining the final expression of the dissipative terms is a lengthy process and only the final result along with the key assumptions are stated here. The reader is referred to Appendix A for the details of the derivation. The system of equations with the dissipative terms is as follows:

$$\begin{cases} \partial_t \left(\rho \right) + \partial_x \left(\rho u \right) = \partial_x \left(\kappa \partial_x \rho \right) \\ \partial_t \left(\rho u \right) + \partial_x \left(\rho u^2 + P + \frac{\epsilon}{3} \right) = \partial_x \left(\kappa \partial_x \rho u \right) \\ \partial_t \left(\rho E \right) + \partial_x \left[u \left(\rho E + P \right) \right] + \frac{u}{3} \partial_x \epsilon = \partial_x \left(\kappa \partial_x (\rho E) \right) \\ \partial_t \epsilon + \frac{4}{3} \partial_x \left(u \epsilon \right) - \frac{u}{3} \partial_x \epsilon = \partial_x \left(\kappa \partial_x \epsilon \right) \end{cases}, \tag{7}$$

where κ is a locally defined positive viscosity coefficient. It was assumed that

the following conditions hold:

$$\begin{cases} P\frac{\partial s}{\partial e} + \rho^2 \frac{\partial s}{\partial \rho} + \frac{4}{3}\rho\epsilon\frac{\partial s}{\partial \epsilon} = 0 \\ s(\rho, e, \epsilon) = s(\rho, e)_{Euler} + s(\epsilon, \rho)_{rad} = s(\rho, e)_{Euler} + \frac{\rho^{(0)}}{\rho}\epsilon^{\frac{3}{4}} \end{cases} \tag{8}$$

where s_{rad} is concave with respect to the radiation energy density ϵ and s_{Euler} is concave with respect to the internal energy e and the specific volume ρ^{-1}. The constant $\rho^{(0)}$ appears for dimensionality purposes and will be derived further in Section 2.2 when performing an asymptotic study to derive the equilibrium-diffusion equations.

2.2. The equilibrium-diffusion limit

We now perform an asymptotic limit onto the 1-D Grey non-equilibrium diffusion Radiation-Hydrodynamic equations modified with the viscous regularization derived in Section 2.1 to investigate whether we recover the correct asymptotic equations and to compare them against the equilibrium-diffusion radiation-hydrodynamic equations taken from Section 4 of [10]. The equations with the viscous regularization derived in Section 2.1 are recalled:

$$\begin{cases} \partial_t(\rho) + \partial_x(\rho u) = \vec{\nabla}\cdot\left(\kappa\vec{\nabla}\rho\right) \\ \partial_t(\rho u) + \partial_x\left(\rho u^2 + P + \frac{\epsilon}{3}\right) = \vec{\nabla}\cdot\left(\kappa\vec{\nabla}(\rho u)\right) \\ \partial_t(\rho E) + \partial_x\left[u(\rho E + P)\right] = -\frac{u}{3}\partial_x\epsilon - \sigma_a c\left(aT^4 - \epsilon\right) + \vec{\nabla}\cdot\left(\kappa\vec{\nabla}(\rho E)\right) \\ \partial_t\epsilon + \frac{4}{3}\partial_x(u\epsilon) = \frac{u}{3}\partial_x\epsilon + \partial_x\left(\frac{c}{3\sigma_t}\partial_x\epsilon\right) + \sigma_a c\left(aT^4 - \epsilon\right) + \vec{\nabla}\cdot\left(\kappa\vec{\nabla}\epsilon\right) \end{cases}. \tag{9}$$

To derive the scaled version of Eq. (9), we consider the following non-dimensionalization:

$$\rho' = \frac{\rho}{\rho_\infty},\ u' = \frac{u}{u_\infty},\ P' = \frac{P}{\rho_\infty c_{m,\infty}^2},\ \epsilon' = \frac{\epsilon}{aT_\infty^4},\ E' = \frac{E}{c_{m,\infty}^2},\ \sigma_t' = \frac{\sigma_t}{\sigma_{t,\infty}},$$
$$\sigma_a' = \frac{\sigma_a}{\sigma_{a,\infty}},\ T' = \frac{T}{T_\infty},\ x' = \frac{x}{L_\infty},\ t' = \frac{t}{L_\infty/u_\infty},\ \kappa' = \frac{\kappa}{\kappa_\infty}, \tag{10}$$

where the subscript ∞ denote the far-field or stagnation quantities and the superscript $'$ stands for the non-dimensional variables. The far-field reference quantities are chosen such that the dimensionless flow quantities are of order

one. Using the scaled variables introduced in Eq. (10), the non-dimensionalized equations are obtained:

$$\begin{aligned}
\partial_{t'}\left(\rho'\right)+\partial_{x'}\left(\rho' u'\right) &= \mathrm{P\acute{e}}_{\infty}\vec{\nabla}\cdot\left(\kappa'\partial_{x'}\rho'\right)\\
\partial_{t'}\left(\rho' u'\right)+\partial_{x'}\left(\rho u^{2'}+P'+\frac{\epsilon'}{3}\right) &= \mathrm{P\acute{e}}_{\infty}\partial_{x'}\left(\kappa'\partial_{x'}(\rho' u')\right)\\
\partial_{t'}\left(\rho' E'\right)+\partial_{x'}\left[u'\left(\rho' E'+P'\right)\right] &= -\frac{u'}{3}\partial_{x'}\epsilon'-\\
&\quad \mathrm{Re}_{\infty}\mathrm{U}_{\infty}^{-1}\mathrm{L}_{\infty}\left(\sigma_t'-\mathrm{L}_{s,\infty}\sigma_a'\right)\left(T^{4'}-\epsilon'\right)+\mathrm{P\acute{e}}_{\infty}\partial_{x'}\left(\kappa'\partial_{x'}(\rho' E')\right)\\
\partial_{t'}\epsilon'+\frac{4}{3}\partial_{x'}\left(u'\epsilon'\right) &= \frac{u'}{3}\partial_{x'}\epsilon'+\mathrm{L}_{\infty}\mathrm{U}_{\infty}^{-1}\partial_{x'}\left(\frac{1}{3\sigma_t'}\partial_{x'}\epsilon'\right)+\\
&\quad \mathrm{Re}_{\infty}\mathrm{U}_{\infty}^{-1}\mathrm{L}_{\infty}\left(\sigma_t'-\mathrm{L}_{s,\infty}\sigma_a'\right)\left(T^{4'}-\epsilon'\right)+\mathrm{P\acute{e}}_{\infty}\partial_{x'}\left(\kappa'\partial_{x'}\epsilon'\right)\ ,
\end{aligned} \tag{11}$$

where:

$$\mathrm{L}_{\infty}=\frac{\sigma_{t,\infty}}{L_{\infty}}\ ,\mathrm{L}_{s,\infty}=\frac{\sigma_{t,\infty}}{\sigma_{a,\infty}}\ ,\mathrm{U}=\frac{c_{m,\infty}}{c}\ ,$$
$$\mathrm{Re}_{\infty}=\frac{aT_{\infty}^{4}}{\rho_{\infty}u_{\infty}^{2}}\ \text{and}\ \mathrm{P\acute{e}}_{\infty}=\frac{\kappa_{\infty}}{u_{\infty}L_{\infty}}\ . \tag{12}$$

The number L_{∞} denote the ratio of the spatial characteristic spatial scale length of the radiation-hydrodynamic solution to the radiation mean-free-path and is scaled $O(1)$. $\mathrm{L}_{s,\infty}$ represents the ratio of the total mean-free-path to the scattering mean-free-path and scales as $O(\varepsilon)$. The relativistic effect are measured by the number U_{∞}, and Re_{∞} is a measure of the ratio of the material energy to the radiation energy. They scale as $O(\varepsilon)$ and $O(1)$, respectively. Lastly, the Péchlet number, $\mathrm{P\acute{e}}_{\infty}$, measures the ratio of the viscous term to the advection term and its scaling is chosen so that the equilibrium-diffusion equations are recovered with well-scaled dissipative terms (the equilibrium-diffusion equations can develop shocks and thus, require stabilization terms). The scaling of the Péchlet number can be devised from the scaled continuity equation. Let us assume that $\mathrm{P\acute{e}}_{\infty}$ scales as ε: in that case the leading-order continuity equation does

not have any stabilization terms which will yields to the formation of spurious oscillations in shock regions. The same study will show the same inconsistency when assuming $\text{Pé}_\infty = O(\varepsilon^{-1})$. Thus, the Péchlet number is chosen to a scale as one to yield well-scaled dissipative terms in all of the equations. We assume that each variable is expanded in a power series in ε, e.g.,

$$x = \sum_i x_i \varepsilon^i \ , \tag{13}$$

where x denotes a variable. By substituting the expanded expression of each variable in Eq. (11) and using the scaling of the non-dimensionalizing numbers, the leading-, first- and second-order equations are retrieved. The leading-order of Eq. (11) yields:

$$\begin{aligned} &\partial_t \rho_0 + \partial_x \left(\rho u\right)_0 = \partial_x \left(\kappa \partial_x \left(\rho u\right)\right)_0 \ , \\ &\partial_t \left(\rho u\right)_0 + \partial_x \left(\rho u^2 + P + \frac{\epsilon}{3}\right)_0 = \partial_x \left(\kappa \partial_x \left(\rho u\right)\right)_0 \ , \\ &\epsilon_0 = T_0 \ . \end{aligned} \tag{14}$$

The first-order material energy and radiation equations along with $T_0 = \epsilon_0$ yield: $\epsilon_1 = T_1$. The asymptotic total energy equation is obtained by taking the second-order material and radiation energy equations and summing them to cancel the second-order relaxation terms:

$$\partial_x \left(\rho E^*\right)_0 + \partial_x \left[u \left(\rho E^* + P^*\right)\right] = \partial_x \left(\frac{1}{3\sigma_t} \partial_x \epsilon\right)_0 + \partial_x \left(\kappa \partial_x \epsilon\right)_0$$

where $P^* = P + \text{Re}_\infty^{-1} \frac{T^4}{3}$ and $e^* = e + \text{Re}_\infty^{-1} \frac{T^4}{3\rho}$ are the radiation-modified pressure and internal energy and match the definitions given in [10]. The equilibrium-diffusion system of equations is obtained by taking the leading-order continuity and momentum equations, and the second-order total energy

equation, e.g,

$$
\begin{aligned}
&\partial_t \rho_0 + \partial_x \left(\rho u\right)_0 = \partial_x \left(\kappa \partial_x \left(\rho u\right)\right)_0 \ , \\
&\partial_t \left(\rho u\right)_0 + \partial_x \left(\rho u^2 + P^*\right)_0 = \partial_x \left(\kappa \partial_x \left(\rho u\right)\right)_0 \ , \\
&\partial_x \left(\rho E^*\right)_0 + \partial_x \left[u \left(\rho E^* + P^*\right)\right] = \partial_x \left(\frac{1}{3\sigma_t} \partial_x T^4\right)_0 + \partial_x \left(\kappa \partial_x \rho E^*\right)_0 \ .
\end{aligned}
\tag{15}
$$

The viscous regularization proposed in Section 2.1 conserves the equilibrium-diffusion limit and also ensures the stability of Eq. (15),i.e., by yielding well-scaled dissipative terms in each equation of Eq. (15). Also, when removing the diffusion term, $\partial_x \left(\frac{1}{3\sigma_t} \partial_x T^4\right)_0$, Eq. (15) yields a hyperbolic system of equations stabilized by a parabolic regularization [14] which ensures that the entropy minimum principle holds.

We also investigate how the asymptotic limit affects the entropy function $s(\rho, e, \epsilon)$, given in Eq. (8) and derived from the hyperbolic terms of the 1-D grey non-equilibrium RHD. We first derive the non-dimensionalized entropy by scaling the entropy with $\frac{\rho_\infty c_{m,\infty}^2}{T_\infty}$ which yields:

$$
s'\left(\rho', e', \epsilon'\right) = s'\left(\rho', e'\right)_{Euler} + \mathrm{Re}_\infty^{-1} \frac{\rho'^{(0)}}{\rho'} \epsilon^{\frac{3}{4}\prime}
\tag{16}
$$

Remembering that $\mathrm{Re}_\infty = O(1)$ and that $T_0^4 = \epsilon_0$, the leading-order entropy yields (the superscript are omitted again for brevity):

$$
s\left(\rho, e\right)_0 = s\left(\rho, e\right)_{Euler,0} + \frac{\rho^{(0)}}{\rho_0} T_0^4 \ .
\tag{17}
$$

Eq. (17) is to compare against the entropy, s^*, obtained when considering the frozen in limit of the equilibrrium-diffusion limit and the Radiation Equation of State (REOS) introduced in Section 4 of [10], e.g.:

$$
s^*(\rho, e) = s(\rho, e)_{Euler} + \frac{4T^3}{3\rho} \ .
\tag{18}
$$

The difference between the two entropy expressions given in Eq. (18) and Eq. (17)

lies in the parameter $\rho^{(0)}$ that is remained to determine. In order to make s_0 and s^* equal in the equilibrium-diffusion limit, $\rho^{(0)}$ is set to $\frac{4}{3}$ which yields the following *dimensionalized* entropy:

$$s\left(\rho, e, \epsilon\right) = s\left(\rho, e\right)_{Euler} + \frac{4}{3\rho}\left(\frac{\epsilon}{a}\right)^{\frac{3}{4}} \tag{19}$$

Eq. (19) can be used to recast the radiation contribution to the definition of the speed of sound given in Eq. (5) under the form of a partial derivative alike the definition of the speed of sound for the pure Euler equations. Using the definition of the radiation entropy, s_{rad}, it can be shown that:

$$c_{rad}^2 = \frac{4\epsilon}{9\rho} = \left.\frac{\partial P_{rad}}{\partial \rho}\right|_{s_{rad}}, \tag{20}$$

where $P_{rad} = \frac{\epsilon}{3}$ is a radiation pressure. Using Eq. (20), the speed of sound c_m^2 can be rewritten as follows:

$$c_m^2 = c_{Euler}^2 + c_{rad}^2 = \left.\frac{\partial P}{\partial \rho}\right|_{s_{Euler}} + \left.\frac{\partial P_{rad}}{\partial \rho}\right|_{s_{rad}} \tag{21}$$

have to add something about c_m being the upper bound of the sound speed definition introduced in [10] In this section, we demonstrated that the viscous regularization derived for the hyperbolic terms of the 1-D grey non-equilibrium radiation-hydrodynamic equations yields the correct asymptotic limit in the equilibrium-diffusion limit, and that the entropy function $s(\rho, e, \epsilon)$ degenerate to the entropy s^* introduced in [10] in the leading-order. Also, we were able to recast the definition of the sound speed in terms of partial derivatives and by introducing the radiative pressure P_{rad}.

2.3. A definition for the viscosity coefficients

Once the dissipative terms are obtained, it remains to define the local viscosity coefficient $\kappa(x, t)$. Following the methodology used in [2, 3], we require the following to hold in the prescription for κ:

- Since the entropy residual is a measure of the entropy production that occurs in shock regions, it is natural to define a viscosity coefficient proportional to the entropy residual. This will enable shock detection and tracking and will also provide a measure of the viscosity required to stabilize the scheme. This viscosity coefficient is referred to as the *entropy viscosity coefficient* or *second-order viscosity coefficient* and is denoted by $\kappa_e(x,t)$.

- An upper bound on κ is to be set since entropy production can be very large in shocks. For explicit time integration, the maximum value of the viscosity coefficient is related to the Courant-Friedrichs-Lewy number (CFL). The upper bound on κ is defined by analogy to the standard upwind (Godunov) scheme that is known to efficiently smooth out oscillations (but is only first-order accurate). With implicit temporal integrators, the same reasoning is used even if the CFL number may not need to be strictly respected. This upper bound will be referred to as the *first-order viscosity*, denoted by $\kappa_{max}(x,t)$.

- The viscosity coefficient κ that is actually used in the dissipative terms of Eq. (3) is defined as follows: $\kappa(x,t) = \min(\kappa_e(x,t), \kappa_{max}(x,t))$. With such a definition, the viscosity added to the system of equations will saturate to the first order viscosity in the shock regions. Elsewhere, the entropy production and thus the viscosity coefficient κ are expected to be small.

Next, we define the local first- and second-order viscosity coefficients $\kappa_{max}(x,t)$ and $\kappa_e(x,t)$, respectively. Following the work of Zingan et al. [9], the first-order viscosity definition is based on the local largest eigenvalue that is known to be $|u| + c_m$ in 1-D:

$$\kappa_{max} = \frac{h}{2}\left(|u| + c_m\right) \tag{22}$$

where h is the local grid size. This definition is derived based on the upwind scheme and a simple derivation can be found in [2] in the case of a scalar hyperbolic equation. Through the definition of the radiation-modified speed of

sound c_m, both the material and radiation properties are accounted for in the definition of the first-order viscosity coefficient.

The definition of the second order viscosity coefficient $\kappa_e(x,t)$ is based upon the entropy residual (Eq. (6)) recast as a function of pressure P, density ρ and radiation energy density ϵ:

$$\tilde{D}_e(x,t) = \frac{s_e}{P_e} \underbrace{\left(\frac{dP}{dt} - c^2_{Euler} \frac{d\rho}{dt} \right)}_{\hat{D}_e(x,t)} \tag{23}$$

The term s_e is the inverse of the material temperature (Appendix A) and P_e is computed from the IGEOS. These two terms are positive so that the sign of the entropy residual $\tilde{D}_e(x,t)$ can be determined by simply inspecting the terms inside the parentheses, denoted by $\hat{D}_e(x,t)$. Such an expression is easier to compute than the one given in Eq. (6) which required an analytical expression for the entropy function. In addition to the entropy residual, inter-element jumps in the pressure and density gradients, J, are also accounted for. The objective is to be able to also detect discontinuities that are not shocks, such as contact waves (there is no entropy production in a contact wave), in order to stabilize them as well.

Thus, the entropy viscosity coefficient $\kappa_e(x,t)$ is set to be proportional to $\hat{D}_e(x,t)$ and J with the following form:

$$\kappa_e(x,t) = h^2 \frac{\max(|\hat{D}_e(x,t)|, J)}{\text{norm}_P} \tag{24}$$

where $J = \max_i(J(x_i,t))$, and $J(x_i,t)$ is the jump of a given quantity at cell interface x_i, and norm_P is a normalization function (of the same units as pressure) that has to be chosen so that the viscosity coefficient κ has units of m^2/s and to ensure the correct asymptotic equations in the equilibrium-diffusion limit. Using the definition of the viscosity coefficient given in Eq. (24) and the scaling

of Eq. (10), it can be shown that:

$$\kappa_\infty = \frac{\rho_\infty c_{m,\infty}^2 u_\infty L_\infty}{\text{norm}_{P,\infty}} \ . \tag{25}$$

The scaling of the viscosity coefficient, κ_∞, is tied to the Péchlet number defined in Eq. (12) that was proved to scale as one in order to preserve the equilibrium-diffusion limit. Thus, using the definition of the Péchlet number and the expression for κ_∞, it is devised that:

$$\text{norm}_{P,\infty} = \rho_\infty c_{m,\infty}^2 \ ,$$

which leads us to choose: $\text{norm}_P = \rho c_m^2$. Thus, the final definition for the viscosity coefficient κ is the following:

$$\kappa_e(x,t) = h^2 \frac{\max(|\hat{D}_e(x,t)|, J)}{\rho c_m^2} \ . \tag{26}$$

The jump J in the definition of $\kappa(x,t)$ is piecewise-constant. Its definition is discretization-dependent and defined as follows for Continuous Galerkin FEM:

$$\begin{cases} J_P(x_i,t) = |u|[[\partial_x P]] \\ J_\rho(x_i,t) = c_m^2 |u|[[\partial_x \rho]] \\ J(x_i,t) = \max(J_\rho(x_i,t), J_P(x_i,t)) \end{cases} \tag{27}$$

The symbol $[[\cdot]]$ denotes the jump at the cell interface.

The entropy viscosity method is now well defined for the hyperbolic system given in Eq. (3) and will be used to solve for the grey radiation-hydrodynamic equations given in Eq. (1). However, one may question how the relaxation source terms, $\sigma_a c(aT^4 - \epsilon)$ and the physical diffusion term, $\partial_x(D\partial_x\epsilon)$, may affect the entropy viscosity method. When applying the entropy viscosity method, the radiation energy density equation will now contain a diffusive term and a numerical dissipative term with a vanishing viscosity coefficient κ. As long as the diffusive coefficient $D = \frac{c}{3\sigma_t}$ is larger than the viscosity coefficient κ, the

numerical dissipative term should not be required. A way to ensure consistency and prevent the formation of oscillations in the frozen limit is to merge the two second-order derivative terms into one as follows:

$$\partial_x \left(\frac{c}{3\sigma_t} \partial_x \epsilon \right) + \partial_x \left(\kappa \partial_x \epsilon \right) \Longrightarrow \partial_x \left[\max \left(\frac{c}{3\sigma_t}, \kappa \right) \partial_x \epsilon \right] \tag{28}$$

Thus, as long as the artificial viscosity coefficient κ is locally smaller that the physical diffusive coefficient $D = \frac{c}{3\sigma_t}$, no artificial viscosity is required to ensure stability of the numerical scheme. As the diffusive coefficient D goes to zero, shocks can form in the radiation energy density profile and will require a certain amount of viscosity in order to prevent oscillations from appearing.

The effect of the relaxation source terms onto the entropy viscosity method can become problematic in the equilibrium diffusion limit ($\sigma_a c \to \infty$): the relaxation source terms behave as dissipative terms and make the system parabolic [4]. In [15], a study on the impact of various artificial viscosity methods onto hyperbolic systems with relaxation terms was carried out. It was shown that high-order viscosity coefficients are more suitable since they do not alter the physical solution as much as first-order viscosity terms (upwind scheme). A manufactured solution is employed in Section 4.1 to test the convergence of the numerical solution in the equilibrium-diffusion limit.

Remark 2.1. *The normalization factor has to be larger than h in order to conserve high-order accuracy.*

Remark 2.2. *The reader will notice that, except for the definition of the jumps, the whole method is independent of the spatial discretization employed. The technique could be used with discontinuous Galerkin finite element or finite volume methods. In both cases, an adequate definition of the jump terms can be found in [9].*

3. Numerical scheme and solution technique

The 1-D radiation-hydrodynamic equations Eq. (1) are discretized with the continuous Galerkin finite element method (CGFEM) under the MOOSE framework [16]. To obtain a weak form, the following generic form of Eq. (1) is considered:

$$\partial_t U + \partial_x F\left(U\right) = S + \partial_x H\left(U\right) \tag{29}$$

where U is the solution vector, F is a conservative vector flux, S is a vector containing the relaxation source terms and non-conservative terms, and H is the artificial viscosity dissipative flux:

$$U = \begin{bmatrix} \rho \\ \rho u \\ \rho E \\ \epsilon \end{bmatrix},\ F(U) = \begin{bmatrix} \rho u \\ \rho u^2 + P + \frac{\epsilon}{3} \\ u\left(\rho E + P\right) \\ \frac{4}{3} u\epsilon \end{bmatrix},\ S = \begin{bmatrix} 0 \\ 0 \\ -\frac{u}{3}\partial_x \epsilon - \sigma_a c\left(aT^4 - \epsilon\right) \\ \frac{u}{3}\partial_x \epsilon + \partial_x\left(\frac{c}{3\sigma_t}\partial_x \epsilon\right) + \sigma_a c\left(aT^4 - \epsilon\right) \end{bmatrix},$$

$$\text{and } H(U) = \begin{bmatrix} \kappa \partial_x \rho \\ \kappa \partial_x (\rho u) \\ \kappa \partial_x \left(\rho e\right) + \frac{u^2}{2}\kappa \partial_x \rho + \rho u \mu \partial_x u \end{bmatrix}$$

In order to apply the continuous finite element method, Eq. (29) is multiplied by a test function ϕ, integrated by parts over the discrete mesh Ω bounded by $\partial\Omega$, to obtain a weak solution:

$$\sum_e \int_e \partial_t U \phi - \sum_e \int_e F(U)\partial_x \phi + \int_{\partial\Omega} F(U)\mathbf{n}\phi - \sum_e \int_e S\phi + \sum_e \int_e H(U)\partial_x \phi - \int_{\partial\Omega} H\left(U\right)\mathbf{n}\phi = 0 \tag{30}$$

where e represents the cells of Ω and $\mathbf{n}$ is the outward normal vector to the boundary of the computational domain.

The integrals over the elements e are evaluated using third-order Gauss quadrature rules. The time-dependent term will be evaluated using the implicit second-order temporal integrator BDF2 [4]. Only linear test functions are considered in

this paper. The integral on $\partial\Omega$ requires computation of the flux $F(U)$ and $H(U)$ on the boundary. It is chosen to treat the boundary for each physics component independently and details will be given in Section 4.2 on how to compute $F(U)$. The viscosity dissipative flux $H(U)$ is zero on the boundaries since the viscosity coefficients κ and μ are set to zero [2, 3, 9].

The Jacobian-Free Newton Krylov method [17] is employed to solve the system for each time step: Newton's and Krylov methods are used for the outer nonlinear and inner linear solves, respectively. The full Jacobian matrix is used as a preconditioner and is computed by finite difference: this is one of the options available in MOOSE and is reasonably efficient for 1-D simulations.

Remark 3.1. *The entropy residual expression is not integrated over the cell volume as it is usually done in the Galerkin finite element method. The variable values and their gradients are available at quadrature points and at different times, and, thus, can be used to evaluate the entropy residual.*

4. Numerical results

In this section, numerical results using the entropy viscosity method are presented for the 1-D grey radiation-hydrodynamic equations. First, second-order accuracy of the method is demonstrated using the method of manufactured solution (MMS). Then, results for some standard radiation-hydrodynamic test cases are given.

4.1. Space/time accuracy

The same manufactured solution as in [7] is used in order to test both the diffusive and streaming limit solutions in a slab of thickness $L = 2\pi\ cm$. The manufactured solutions are composed of trigonometric functions. Periodic boundary conditions are used for all of the variables. The L_2 norm of the error between the numerical and exact solutions are computed for density, momentum, total material energy, and radiation energy density. For each new simulation, the time step is divided by two and the number of spatial degrees of freedom is

doubled. With such settings, the error is expected to decrease by a factor 4 if second-order convergence is achieved.

The first manufactured solution is designed to test the equilibrium-diffusion limit. In that case, the radiation energy is in equilibrium with the material temperature and the opacity is large which means that the radiation mean-free path is not resolved but the variation of the solution is resolved. The following exact solution was used:

$$\begin{cases} \rho = \sin(x-t) + 2 \\ u = \cos(x-t) + 2 \\ T = \frac{0.5\gamma(\cos(x-t)+2)}{\sin(x-t)+2} \\ \epsilon = aT^4 \end{cases} . \tag{31}$$

The cross sections σ_a and σ_t are assumed constant and set to the same value 1000 cm^{-1}. The simulation is run until $t = 3$ sh (1 $sh = 10^{-8}$ sec). The L_2 error norm along with its ratio between consecutive simulations are given in Table 1 for the equilibrium diffusion limit case.

Table 1: L_2 norms of the error for for the equilibrium diffusion limit case using a manufactured solution.

# of cells	time step size (sh)	ρ	**ratio**	ρ**E**	**ratio**
20	10^{-1}	0.590766	NA	1.333774	NA
40	$5\ 10^{-1}$	0.290626	2.03	0.478819	2.79
80	$2.5\ 10^{-2}$	0.0959801	3.021	0.154119	3.11
160	$1.25\ 10^{-2}$	0.02593738	3.70	0.0405175	3.80
320	$6.25\ 10^{-3}$	$6.471444\ 10^{-3}$	4.00	$9.90446\ 10^{-3}$	4.09
640	$3.125\ 10^{-3}$	$1.584158\ 10^{-3}$	4.01	$2.44727\ 10^{-3}$	4.04
# of cells	time step size (sh)	ϵ	**ratio**	ρ**u**	**ratio**
20	10^{-1}	0.00650085	NA	0.910998	NA
40	$5\ 10^{-1}$	0.00124983	5.20	0.4090946	2.23
80	$2.5\ 10^{-2}$	0.000262797	4.76	0.125943	3.25
160	$1.25\ 10^{-2}$	$6.17726\ 10^{-5}$	4.25	$3.381042\ 10^{-3}$	3.72
320	$6.25\ 10^{-3}$	$1.509184\ 10^{-5}$	4.09	$8.373657\ 10^{-3}$	4.04
640	$3.125\ 10^{-3}$	$3.72548\ 10^{-6}$	4.05	$2.070538\ 10^{-3}$	4.04

The second manufactured solution is used to test the method in the streaming limit: the radiation streaming dominates the absorption/re-emission term and evolves at a fast time scale. The exact solution used is as follows :

$$\begin{cases} \rho = \sin(x-t)+2 \\ u = (\sin(x-t)+2)^{-1} \\ T = 0.5\gamma \\ \epsilon = \sin(x-1000t)+2 \end{cases} \tag{32}$$

For this manufactured solution, the cross sections are still assumed constant and set to the same value 1 cm^{-1}. The final time is $t_{final} = 3\ sh$. Once again, the L_2 error norm is given in Table 2 for the density, momentum, material total energy and radiation energy density.

Table 2: L_2 norms of the error for for the streaming limit case using a manufactured solution.

# of cells	time step size (sh)	ρ	**ratio**	$\rho\mathbf{E}$	**ratio**
20	10^{-1}	$1.4373\ 10^{-2}$	NA	$5.88521\ 10^{-1}$	NA
40	$5.\ 10^{-2}$	$3.760208\ 10^{-3}$	3.82	$1.4244\ 10^{-1}$	4.13
80	$2.5\ 10^{-2}$	$9.91724\ 10^{-4}$	3.79	$3.2047\ 10^{-2}$	4.44
160	$1.25\ 10^{-2}$	$2.4455\ 10^{-4}$	4.06	$7.4886\ 10^{-3}$	4.28
320	$6.25\ 10^{-3}$	$6.280715\ 10^{-5}$	3.89	$1.82327\ 10^{-3}$	4.11
640	$3.125\ 10^{-3}$	$1.57920\ 10^{-5}$	3.98	$4.50463\ 10^{-4}$	4.05
1280	$1.5625\ 10^{-4}$	$3.96096\ 10^{-6}$	3.99	$1.12061\ 10^{-4}$	4.02
# of cells	time step size (sh)	ϵ	**ratio**	$\rho\mathbf{u}$	**ratio**
20	10^{-1}	$3.82001\ 10^{-1}$	NA	$2.354671\ 10^{-3}$	NA
40	$5.\ 10^{-2}$	$1.21500\ 10^{-1}$	3.14	$6.138814\ 10^{-4}$	3.84
80	$2.5\ 10^{-2}$	$3.27966\ 10^{-2}$	3.70	$1.74974\ 10^{-4}$	3.51
160	$1.25\ 10^{-2}$	$8.38153\ 10^{-3}$	3.91	$3.61297\ 10^{-5}$	4.84
320	$6.25\ 10^{-3}$	$2.10925\ 10^{-3}$	3.97	$9.03866\ 10^{-6}$	3.99
640	$3.125\ 10^{-3}$	$5.28472\ 10^{-4}$	3.99	$2.25649\ 10^{-6}$	4.01
1280	$1.5625\ 10^{-4}$	$1.322268\ 10^{-4}$	3.99	$5.69984\ 10^{-7}$	3.95

For both manufactured solutions the error is divided by four as the time step and the spatial mesh are reduced by a factor two. Thus, we conclude that GRH equations can be numerically solved with second-order accuracy using the entropy viscosity method when the exact solution is smooth.

4.2. Radiation shock simulations

The purpose of this section is to show that the entropy-based viscosity method (Section 2) can accurately resolve shocks occurring in radiation-hydrodynamic simulations. Multiple test cases are considered, with Mach numbers of 1.05, 1.2, 2, 5 and 50 [11]. All of the simulations are run with 500 spatial cells and with a Courant-Friedrichs-Lewy (CFL number) of 10 until steady-state (even if the

scheme employed here is fully implicit, a CFL number can still be computed and is a good reference for comparison against semi-implicit or fully explicit codes). Linear Lagrange polynomials and the second-order temporal integrator BDF2 are once again used. For clarity, the initial conditions for each test case will be recalled in a table and plots of the density, $\rho(x)$, the radiation temperature, $\theta(x)$, and material temperature, $T(x)$, at steady-state will be given as well as those of the viscosity coefficients, $\kappa(x)$ and $\kappa_{max}(x)$. The computational domain consists of a 1-D slab of thickness L. The initial discontinuity between the left and right states is located at x_0 and will be specified for all test cases. For all of the test cases presented in this paper, the cross sections σ_a and σ_t are assumed constant and set to 853.144 cm^{-1} and 390.711 cm^{-1}, respectively, if not otherwise specified. The heat capacity at constant specific volume is set to $C_v = 0.12348\ jerks/(g - keV)$.

For the Mach 2 simulation, results will also be shown when employing only the first-order viscosity ($\kappa(x,t) = \kappa_{max}(x,t)$) in order to show the benefits of using a high-order viscosity coefficient.

The inlet and outlet boundary conditions (BCs) are given next. The Euler equations and radiation equation are considered independently since the latter one is parabolic. At the inlet, the flow is supersonic and, therefore, no physical information exits the system. Thus, Dirichlet boundary conditions can be used. At the outlet, the flow becomes subsonic which requires a particular treatment. Following the work from [18], a static boundary condition is implemented. Only the back pressure is provided and the other variables are computed using the characteristic equations. For the radiation equation, vacuum boundary conditions are used at both inlet and outlet.

4.2.1. An equilibrium diffusion test

For this test, the inlet Mach number is set to 1.05. The radiation field and material are in equilibrium. The initial conditions are given in Table 3. The computational domain is of size $L = 0.08\ cm$ and the initial step is at $x_0 = 0.015$ cm. The numerical solutions at steady state are given in Fig. 1, Fig. 2 and Fig. 3.

Table 3: Initial conditions for Mach 1.05.

	left	right
$\rho\ (g/cm^3)$	1.	1.0749588
$u\ (cm/sh)$	0.1228902	0.1144127
$T\ (keV)$	0.1	0.1049454
$\epsilon\ (jerks/cm^3)$	1.372 10^{-6}	1.6642117 10^{-6}

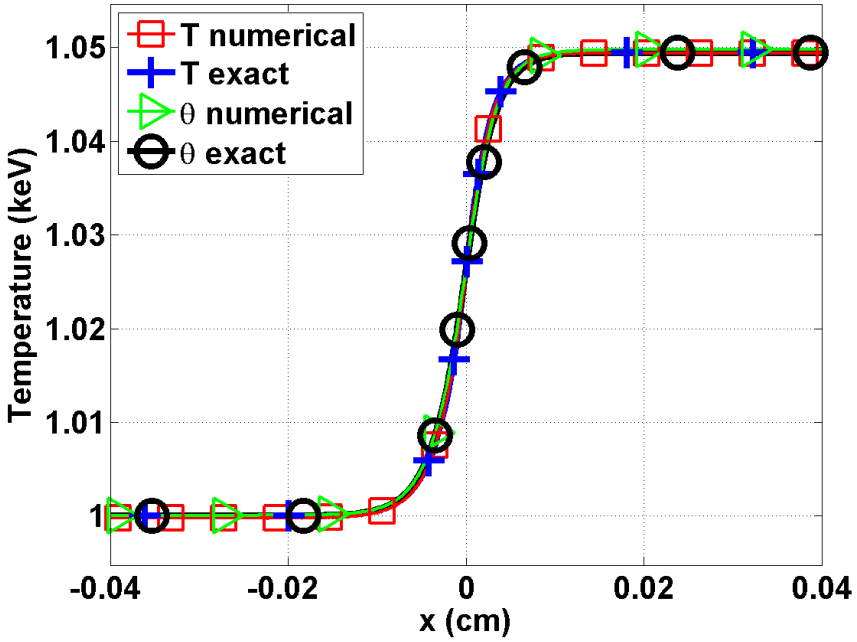

Figure 1: Material and radiation temperature profiles at steady state for Mach 1.05 test.

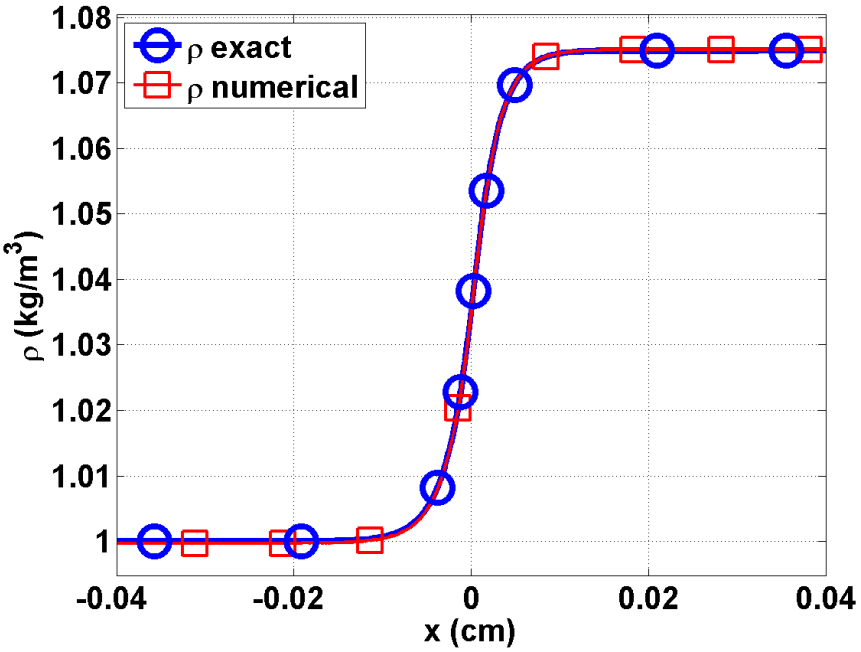

Figure 2: Material density profile at steady state for Mach 1.05 test.

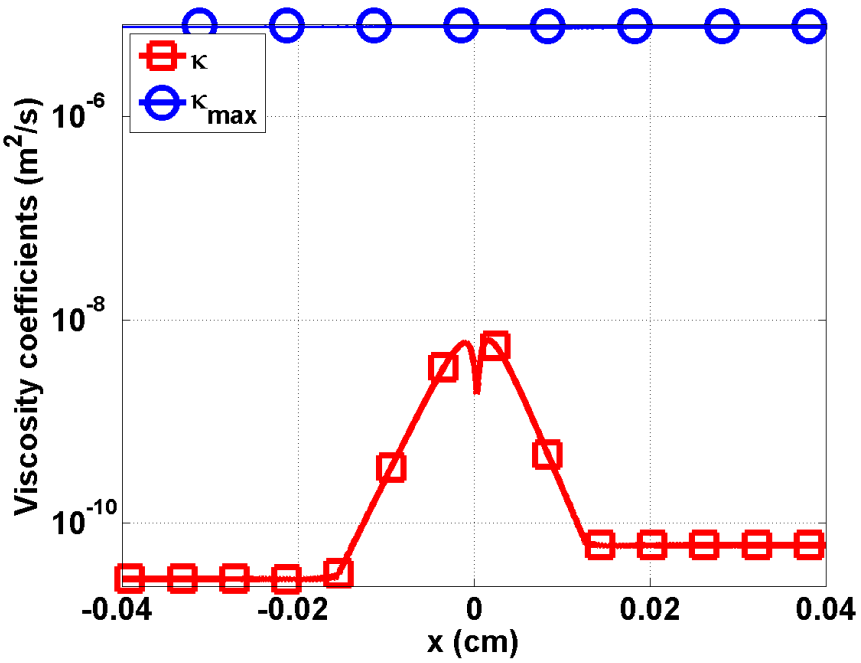

Figure 3: First-order viscosity κ_{max} and second-order viscosity κ profiles at steady state for Mach 1.05 test (logarithm scale).

The energy transfer between the material and radiation fields is not large enough to form a shock in the material. Thus, all of the material variables are smooth (Fig. 1 and Fig. 2) as well as the radiation temperature θ. Because of the smoothness of the solution, the viscosity coefficient κ is three order of magnitude smaller than the first-order viscosity coefficient κ_{max} (Fig. 3).

4.2.2. A 1.2 *Mach hydrodynamic shock*

In this test, the material experiences a shock and the radiation energy density remains smooth. The initial conditions, corresponding to a Mach number of 1.2 at the inlet, are as follows:

Table 4: Initial conditions for Mach 1.2.

	left	right
ρ (g/cm^3)	1.	1.0749588
u (cm/sh)	0.1405588	0.1083456
T (keV)	0.1	0.1194751
ϵ $(jerks/cm^3)$	1.372 10^{-6}	2.7955320 10^{-6}

The slab thickness is set to $L = 0.045$ cm and the initial step was located at $x_0 = 0$ cm.

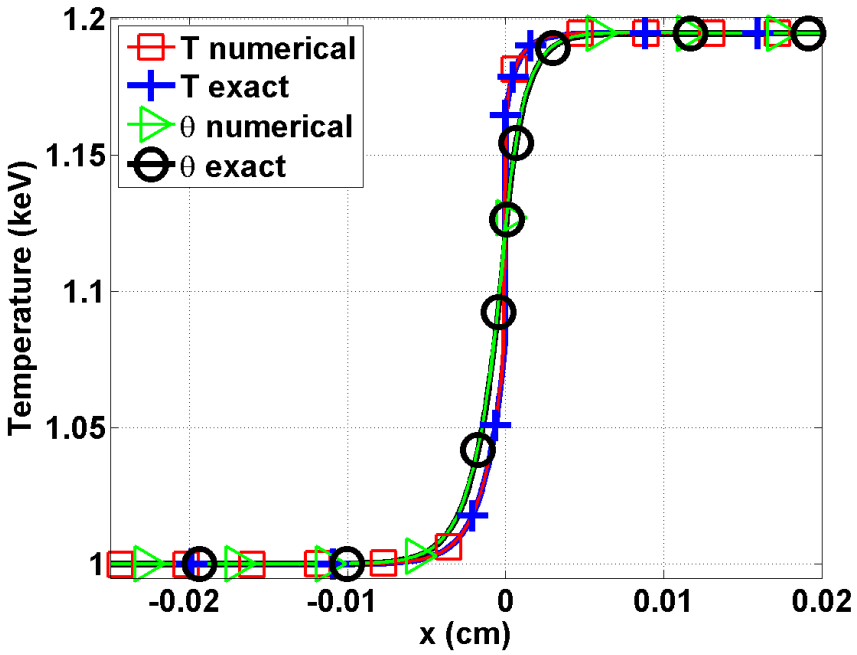

Figure 4: Material and radiation temperature profiles at steady state for Mach 1.2 test.

The radiation and material temperatures have two different behaviors (Fig. 4): the later experiences an embedded hydrodynamic shock, whereas the radiation temperature is smooth because of the diffusion term. The material tempera-

ture profile does not show any pre- and post-shock oscillations. In Fig. 5, the material density profile has a shock as well. The viscosity coefficient (Fig. 6) is peaked in the shock as expected but does not saturate to the first-order viscosity. It is conjectured that the diffusion term in the radiation equation brings extra stability to the system.

Overall, the numerical solution behaves as expected in the shock and the entropy-based viscosity method seems to efficiently stabilize the numerical scheme.

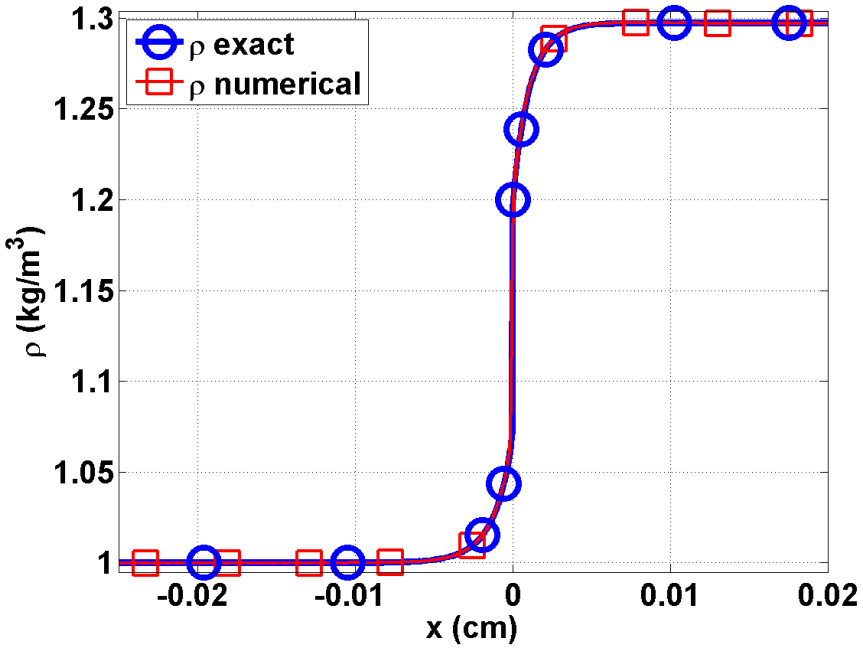

Figure 5: Material density profile at steady state for Mach 1.2 test.

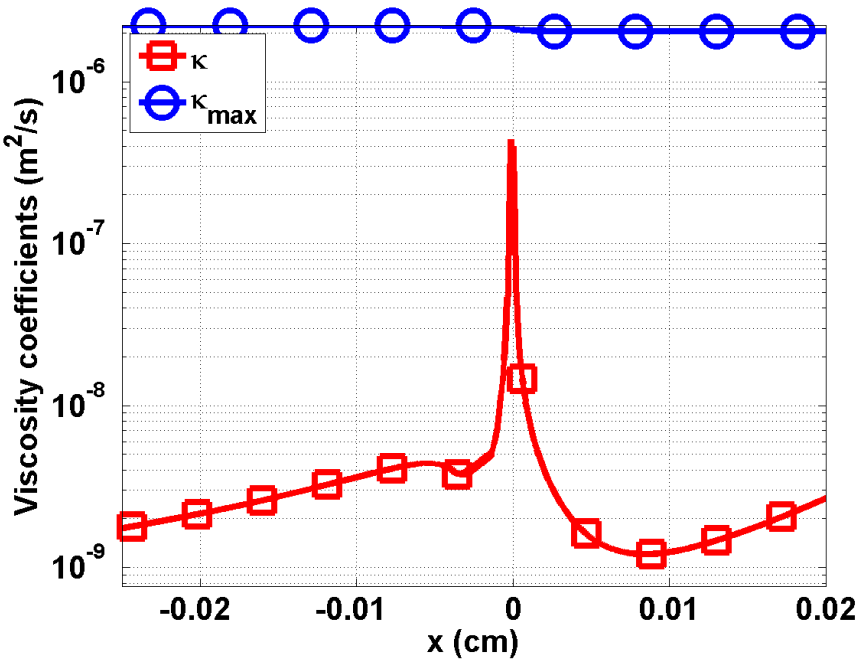

Figure 6: First-order viscosity κ_{max} and second-order viscosity κ profiles at steady state for Mach 1.2 test (logarithm scale).

4.2.3. A Mach 2 shock

The Mach 2 shock test has two features: a hydrodynamic shock and a Zeldovich spike, which make it interesting for testing the robustness of the entropy-based viscosity method. The initial conditions are specified in Table 5 for a slab of length $L = 0.04\ cm$ with $x_0 = 0.\ cm$.

Table 5: Initial conditions for Mach 2.

	left	right
$\rho\ (g/cm^3)$	1.	1.0749588
$u\ (cm/sh)$	0.1405588	0.1083456
$T\ (keV)$	0.1	0.1194751
$\epsilon\ (jerks/cm^3)$	1.372 10^{-6}	2.7955320 10^{-6}

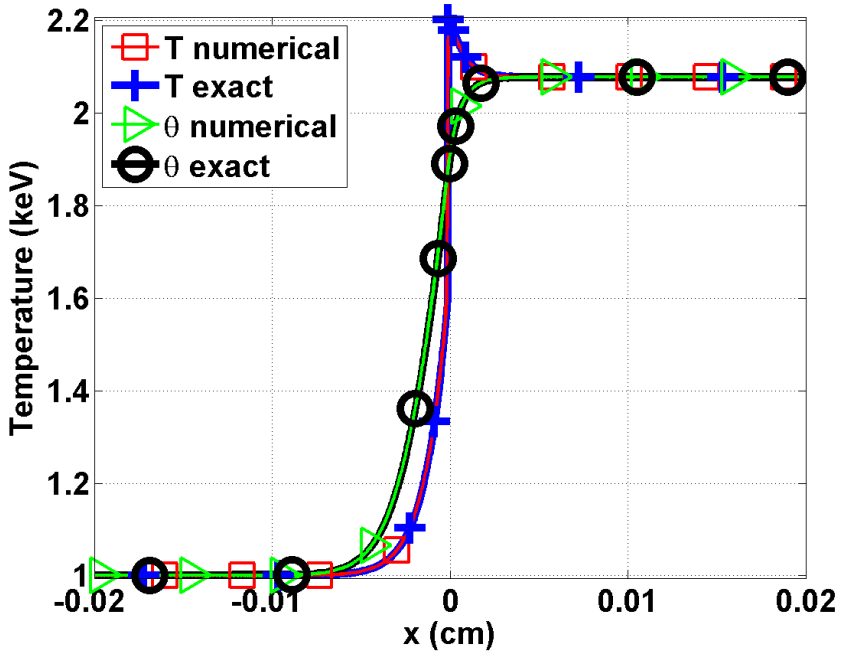

Figure 7: Material and radiation temperature profiles at steady-state for Mach 2 test.

Once again, the radiation temperature profile is smooth and the material temperature experiences an embedded hydrodynamic shock and a peak as shown in Fig. 7. In Fig. 8, the shock is well resolved. The viscosity coefficient profile is given in Fig. 9 and is peaked, once again, in the shock region.

For comparison purpose, the same simulation was run with the first-order viscosity only, i.e., κ was set equal to κ_{max} for the whole domain in order to see the advantage of using a second-order viscosity coefficient. The results are given in Fig. 10 for the material density and temperature. Numerical solutions with first- and second-order viscosity coefficients are graphed. The radiation temperature profile (not shown here) is not affected much by the first-order viscosity and the curves are coincident. This is expected because of the way the artificial viscosity term is treated in the radiation equation (Section 2). However, on the same figure, the shock and peak in the material temperature

profile are smoothed out: the shock is not as sharp and the peak amplitude is reduced because of the larger amount of viscosity added to the system. This test shows the benefits of using a high-order viscosity coefficient in order to avoid over-dissipation.

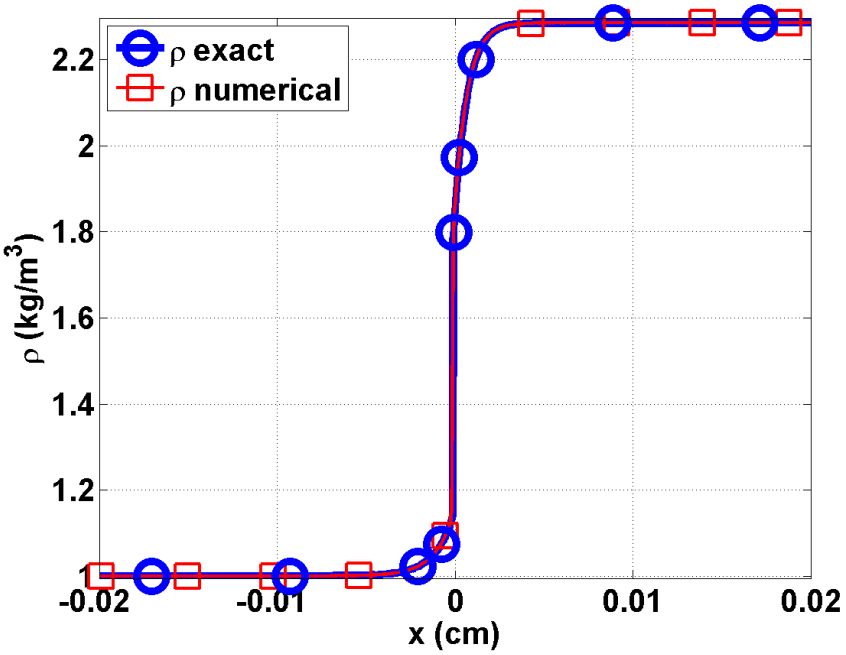

Figure 8: Material density profile at steady-state for Mach 2 test.

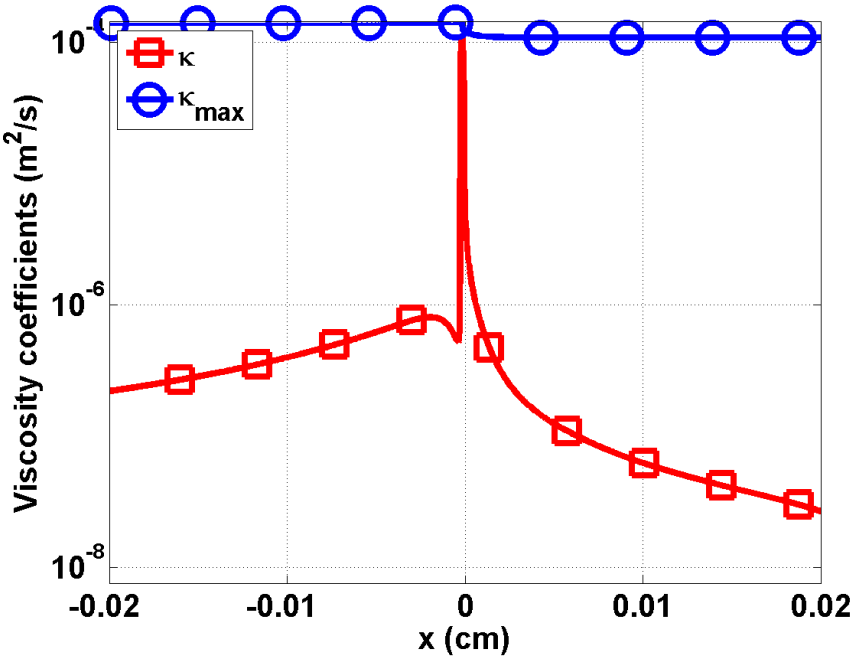

Figure 9: First-order viscosity κ_{max} and second-order viscosity κ profiles at steady state for Mach 2 test.

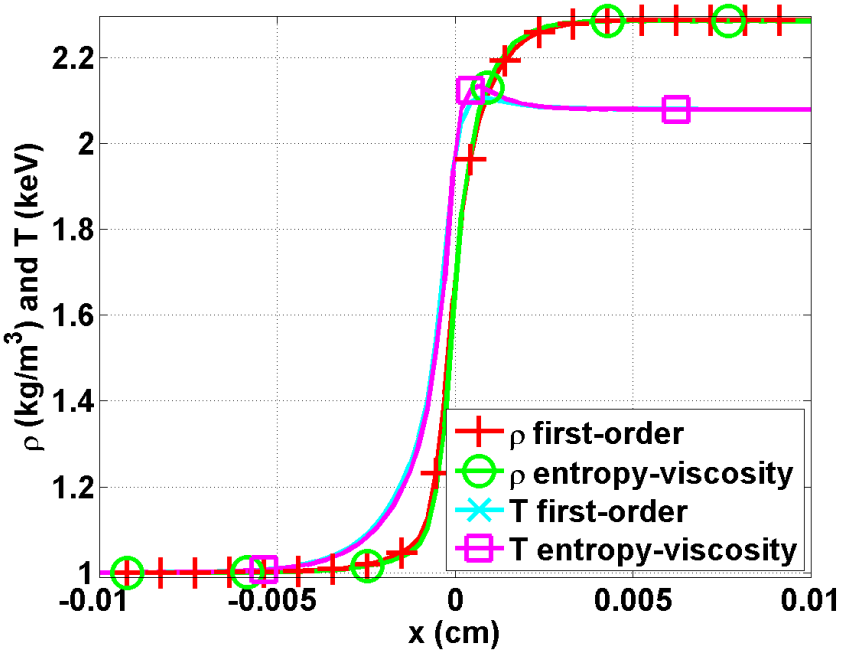

Figure 10: Comprarison between the material density and temperature profiles run with the high-order and first-order viscosity coefficients.

4.2.4. Mach 5 shock

A Mach 5 test is run with the initial conditions of Table 6 on a computational domain of length $L = 0.05\ cm$ ($x_0 = 0\ cm$). Steady-state results are shown in Fig. 11, Fig. 13, and Fig. 14 for the material and radiation temperatures, the density and the viscosity coefficients, respectively.

Table 6: Initial conditions for Mach 5.

	left	right
$\rho\ (g/cm^3)$	1.	1.0749588
$u\ (cm/sh)$	0.1405588	0.1083456
$T\ (keV)$	0.1	0.1194751
$\epsilon\ (jerks/cm^3)$	$1.372\ 10^{-6}$	$2.7955320\ 10^{-6}$

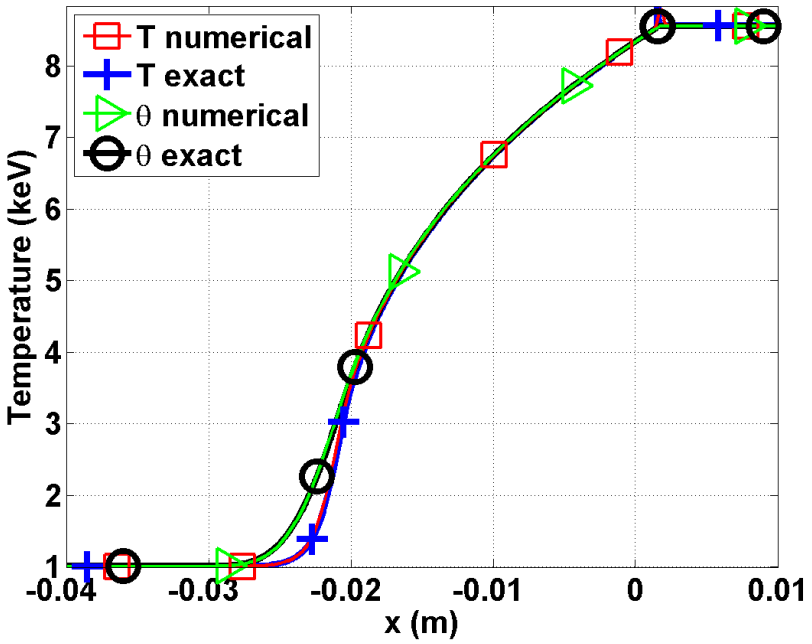

Figure 11: Material and radiation temperature profiles at steady state for Mach 5 test. Zoom at the location go the peak using different mesh resolutions.

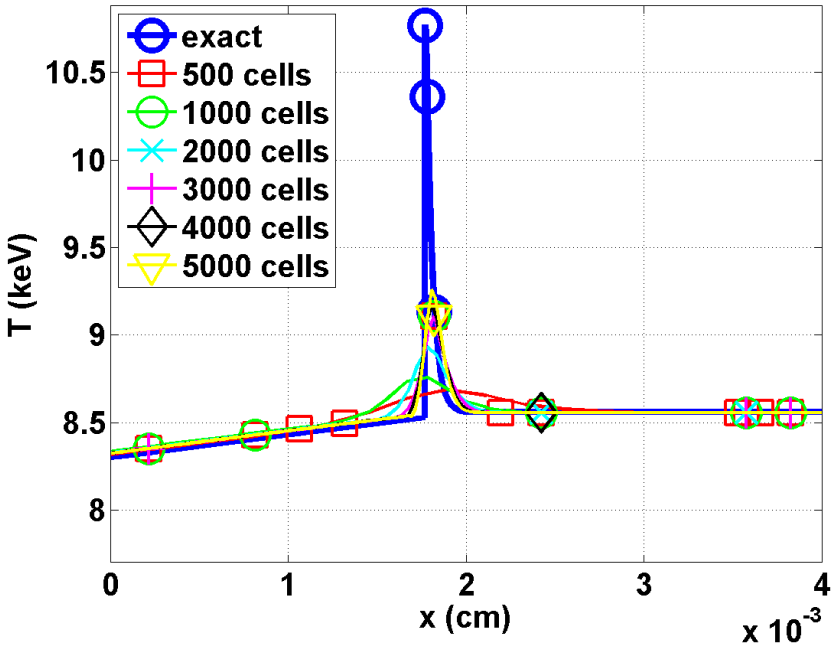

Figure 12: Material temperature profiles at steady state for the Mach 5 test in the neighborhood spike.

In Fig. 11, the radiation temperature profile is smooth. The material temperature no longer exhibits an embedded hydrodynamic shock but shows a Zeldovich spike. The mesh with 500 elements is not fine enough to correctly resolve the Zeldovich spike. In Fig. 12, the Zeldovich spike region is plotted for different mesh resolutions, using from 500 to 5000 elements: the peak is better resolved when using large numbers of elements and its position seems to be independent of the mesh size when appropriately refined. The density profile, Fig. 13, shows a shock located at the same position as the Zeldovich spike of the material temperature profile. The viscosity coefficient κ is also peaked in the shock region, as expected. The material and radiation variables do not present any numerical oscillations.

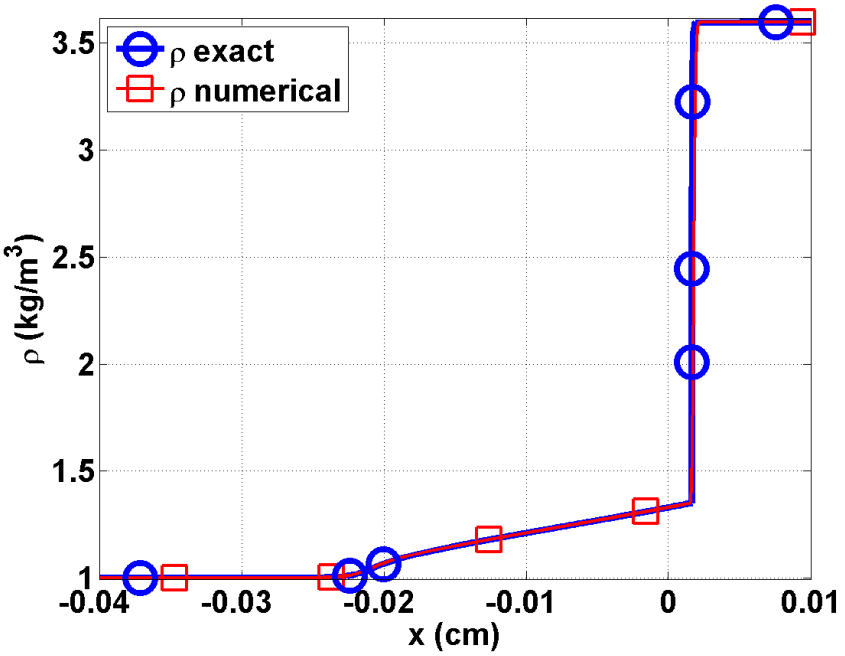

Figure 13: Material density profile at steady state for Mach 5 test.

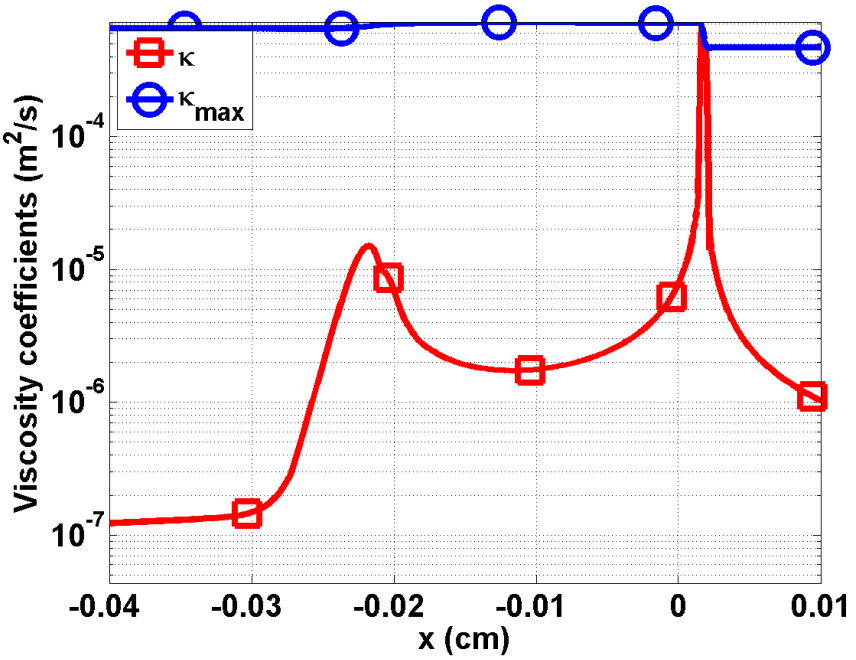

Figure 14: First-order viscosity κ_{max} and second-order viscosity κ profiles at steady state for Mach 5 test.

4.2.5. Mach 50 shock

The Mach 50 test is known to be challenging. The initial conditions are given in Table 7. The computational domain is of length $L = 0.2\ cm$. Results are once again given at steady state.

Table 7: Initial conditions for Mach 50.

	left	right
$\rho\ (g/cm^3)$	1.	6.5189217
$u\ (cm/sh)$	585.6620	89.84031
$T\ (keV)$	1.0	85.51552
$\epsilon\ (jerks/cm^3)$	$1.372\ 10^{-2}$	$7.33726\ 10^5$

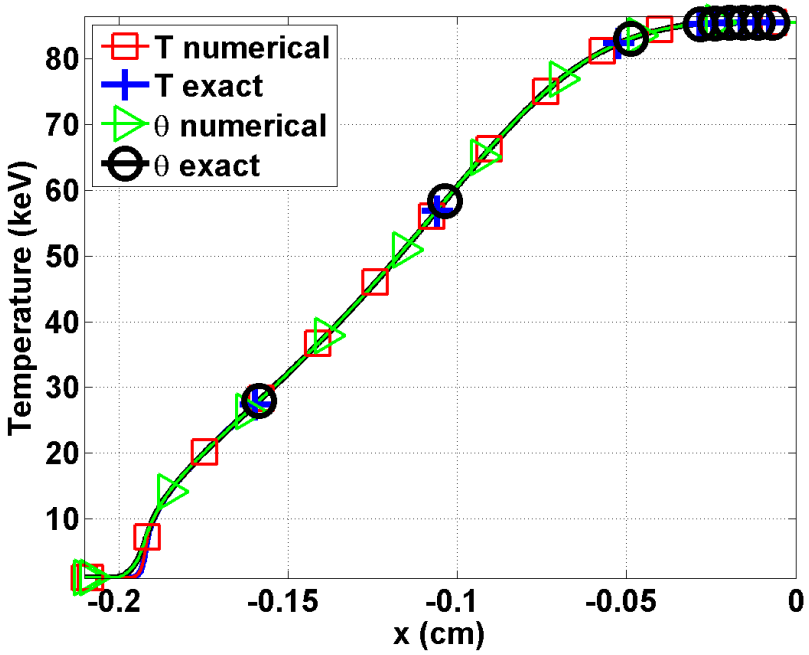

Figure 15: Material and radiation temperature profiles at steady state for Mach 50 test.

At Mach 50, there is no embedded hydrodynamic shock forming as shown in Fig. 15. The density profile is smooth as shown in Fig. 16. In Fig. 15, the material and radiation temperatures overlap on all of the computational domain except for a small region located between $x = -0.2$ and $x = -0.18$ cm. In this particular region, the viscosity coefficient saturates to the first-order viscosity (see Fig. 17) because of the inflection point in the material temperature profile. The artificial dissipative terms correctly stabilize the material temperature profile without altering the physical solution: the radiation temperature is expected to increase ahead of the material temperature.

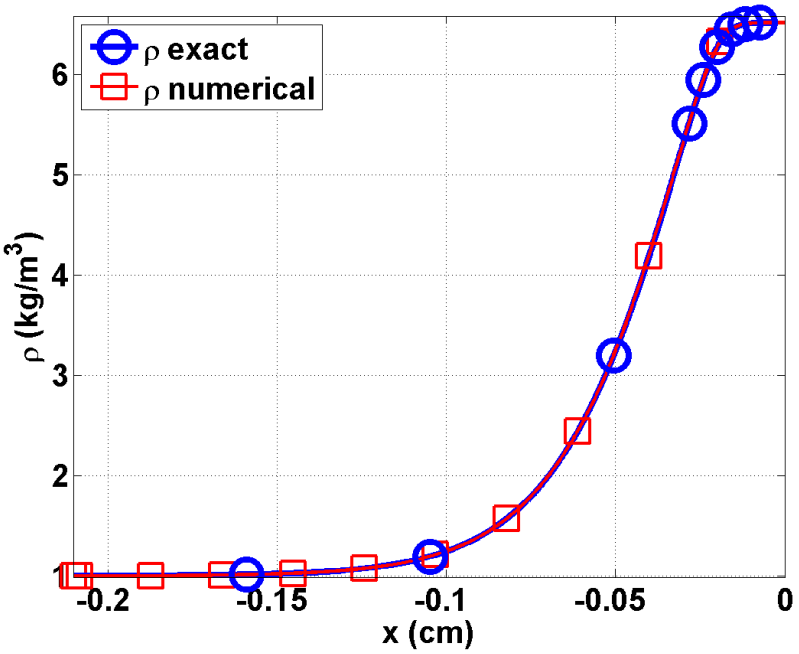

Figure 16: Material density profile at steady-state for Mach 50 test.

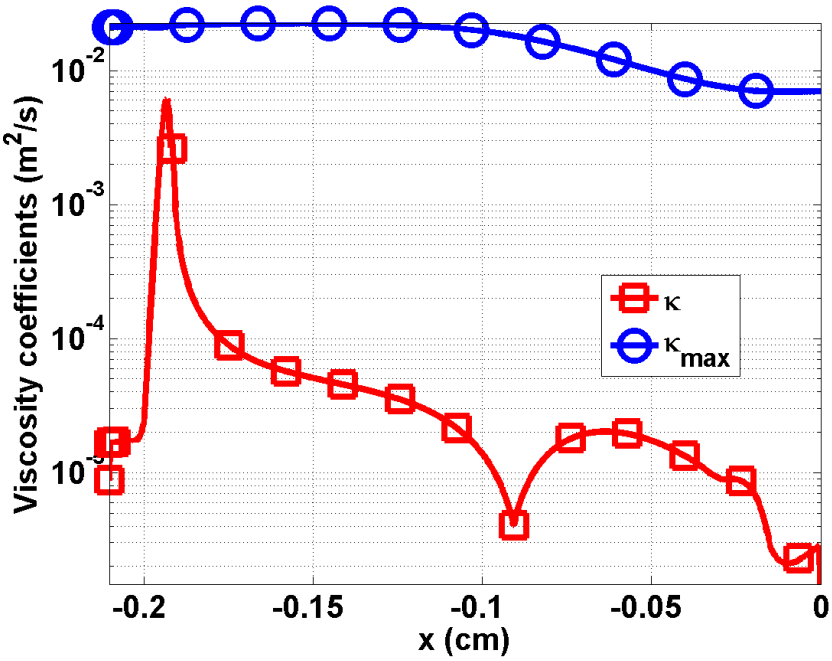

Figure 17: First-order viscosity κ_{max} and second-order viscosity κ profiles at steady-state for Mach 50 test.

5. Conclusions

In this paper, we have shown that the entropy-based viscosity method is a valid candidate for solving the 1-D radiation-hydrodynamic equations. A theoretical derivation is given for the derivation of the dissipative terms that are consistent with the entropy minimum principle. The viscosity coefficient κ is defined proportional to the entropy residual that measures the local entropy production allowing detection of shocks. Through the manufactured solution method, it is demonstrated, firstly, that second-order accuracy is achieved when the solution is smooth, and secondly, that the artificial dissipative terms do not affect the physical solution in the equilibrium-diffusion limit.

The entropy-based numerical scheme also behaves well in the tests performed for Mach numbers ranging from 1.05 to 50. The main features such as the embedded hydrodynamic shock and the Zeldovich spike are resolved accurately

without spurious oscillations. The viscosity coefficient is peaked in the shock region only and behaves as expected. All of these results were obtained by using an unique definition of the viscosity coefficient that is computed on the fly. The addition of dissipative terms to the set of equations requires more computational work but is rather simple to implement.

As future work, extension to the multi-D equations could be considered: all of the derivations presented in this paper hold. The definition of the viscosity coefficients κ and κ_{max} do not need to be modified. It would be interesting to model the radiation equation with an S_n transport approximation and apply the entropy based artificial viscosity to the resultant radiation-hydrodynamics equations. Given the advective nature of the S_n equations, dissipation would need to be added to these equations.

Acknowledgements

The authors would like to acknowledge Jim Ferguson for providing the semi-analytical solutions and Bojan Popov for many fruitful discussions.

A. Proof of the entropy minimum principle for the radiation-hydrodynamic equations with dissipative terms:

In this appendix, a demonstration of the entropy minimum principle for the system of equations Eq. (7) is given. This proof, inspired by [19], details the steps that lead to the derivation of the dissipative terms for the multi-D Euler equations by using the entropy minimum principle.
We start with the hyperbolic system given in Eq. (3) and add dissipative terms to each equation as follows:

$$\begin{cases} \frac{d\rho}{dt} + \rho\partial_x u = \partial_x f \\ \partial_t(\rho u) + \partial_x\left(\rho u^2 + P + \frac{\epsilon}{3}\right) = \partial_x g \\ \partial_t(\rho E) + \partial_x\left[u\left(\rho E + P\right)\right] + \frac{u}{3}\partial_x\epsilon = \partial_x\left(h + ug\right) \\ \partial_t\epsilon + u\partial_x\epsilon + \frac{4}{3}\epsilon\partial_x u = \partial_x l \end{cases} \tag{33}$$

where f, g, h and l are dissipative terms to be determined. Eq. (33) is then recast as a function of the primitive variables (ρ, u, e, ϵ) to yield:

$$\begin{cases} \frac{d\rho}{dt} + \rho\partial_x u = \partial_x f \\ \rho\frac{du}{dt} + \partial_x\left(P + \frac{\epsilon}{3}\right) = \partial_x g - u\partial_x f \\ \rho\frac{de}{dt} + P\partial_x u = \partial_x h + g\partial_x u + \left(0.5u^2 - e\right)\partial_x f \\ \frac{d\epsilon}{dt} + \frac{4}{3}\epsilon\partial_x u = \partial_x l \end{cases} \tag{34}$$

The right-hand side of the internal energy equation can be simplified by choosing the dissipative terms g and h as follows: $h = \tilde{h} - 0.5u^2 f$ and $g = \rho\mu\partial_x u + uf$ where $\mu \geq 0$ is a dissipative coefficient. Using these definitions, the system of equation given in Eq. (34) becomes:

$$\begin{cases} \frac{d\rho}{dt} + \rho\partial_x u = \partial_x f \\ \rho\frac{du}{dt} + \partial_x\left(P + \frac{\epsilon}{3}\right) = \partial_x g - u\partial_x f \\ \rho\frac{de}{dt} + P\partial_x u = \rho\mu(\partial_x u)^2 + \partial_x\tilde{h} - e\partial_x f \\ \frac{d\epsilon}{dt} + \frac{4}{3}\epsilon\partial_x u = \partial_x l \end{cases} \tag{35}$$

This system of equation admits an entropy function s that depends on density ρ, internal energy e and radiation energy density ϵ. In order to prove the entropy minimum principle, a conservation statement satisfied by the entropy is needed. This equation which is referred to as an entropy residual $D_e(x,t)$, can be obtained by a combination of the equations given in Eq. (35). This process is motivated by the following (chain rule)

$$\partial_\alpha s = \partial_\rho s \partial_\alpha \rho + \partial_e s \partial_\alpha e + \partial_\epsilon s \partial_\alpha \epsilon, \tag{36}$$

which holds for any independent variable $\alpha = x, t$. It is also required to define the dissipative terms $\tilde{h}$, f and l. The following definitions are chosen:

$$\begin{cases} f & = \kappa \partial_x \rho \\ \tilde{h} & = \kappa \partial_x (\rho e) \\ l & = \kappa \partial_x \epsilon \end{cases} \tag{37}$$

where κ is another positive dissipative coefficient.

Thus, using the continuity, the internal energy and the radiation equations of Eq. (35) and using Eq. (36) along with the definition of the dissipative terms, a conservation statement satisfied by the entropy s is obtained:

$$\frac{ds}{dt} + \underbrace{\left(P\partial_e s + \rho^2 \partial_\rho s + \frac{4}{3}\rho\epsilon\partial_\epsilon s \right) \partial_x u}_{\text{(a)}} = \partial_x \left(\rho\kappa\partial_x s \right) + \kappa \partial_x \rho \partial_x s - \rho\kappa \underbrace{XAX^t}_{\text{(b)}} + \underbrace{s_e \rho\mu(\partial_x u)^2}_{\text{(c)}} \tag{38}$$

where X is a row vector defined as $X = (\partial_x \rho, \partial_x e, \partial_x \epsilon)$ and A is the 3x3 symmetric matrix:

$$A = \begin{bmatrix} \partial_\rho \left(\rho^2 \partial_\rho s \right) & \partial_{\rho,e} s & \partial_\rho \left(\rho \partial_\epsilon s \right) \\ \partial_{\rho,e} s & \partial_{e,e} s & \partial_{e,\epsilon} s \\ \partial_\rho \left(\rho \partial_\epsilon s \right) & \partial_{e,\epsilon} s & \partial_{\epsilon,\epsilon} s \end{bmatrix} \tag{39}$$

In order to show that an entropy minimum principle holds, the signs of the terms (a), (b) and (c) in Eq. (38) need to be studied.

Regarding (a), it is assumed that $P\partial_e s + \rho^2 \partial_\rho s + \frac{4}{3}\rho\epsilon\partial_\epsilon s = 0$. The motivation

for this is two-fold: First, in order to have a negative sign for the term (a), it would require $P\partial_e s + \rho^2\partial_\rho s + \frac{4}{3}\rho\epsilon\partial_\epsilon s$ to have a sign of opposite to that $\partial_x u$. The thermodynamic variables cannot be a function of the material velocity or its derivative under a non-relativistic assumption. Such a statement would not be true when dealing with relativistic equations of state. Second, a similar assumption was made in [19] for multi-D Euler equations (without the radiation energy): $P\partial_e s + \rho^2\partial_\rho s = 0$.

The term (b), XAX^t, is a quadratic form and its sign is determined by simply looking at the positiveness of the matrix A [20]. Here we need to prove that A is negative-definite which is equivalent to showing the three following inequalities:

$$\begin{cases} A_1 \geq 0 \\ A_2 \leq 0 \\ A_3 = A \geq 0 \end{cases} \tag{40}$$

where A_k is the k^{th} order leading principle minor. Determining the sign of the last inequality that corresponds to the determinant of the 3 by 3 matrix A can be difficult and needs to be simplified. Zeroing out the off-diagonal entries of the last row or column would simplify the expression for the determinant of A. This can be achieved by assuming $\partial_\rho(\rho\partial_\epsilon s)$ and $\partial_{e,\epsilon} s$ are zero, which requires the following form for the entropy function:

$$s(\rho, e, \epsilon) = s_{Euler}(\rho, e) + \frac{\rho^{(0)}}{\rho} s_{rad}(\epsilon). \tag{41}$$

where s_{Euler} and s_{rad} are two functions whose properties will be provided later. Next, using the expression of the entropy given in Eq. (41), matrix A becomes:

$$A = \begin{bmatrix} \partial_\rho\left(\rho^2\partial_\rho s_{Euler}\right) & \partial_{\rho,e} s_{Euler} & 0 \\ \partial_{\rho,e} s_{Euler} & \partial_{e,e} s_{Euler} & 0 \\ 0 & 0 & \rho^{-1}\partial_{\epsilon,\epsilon} s_{rad} \end{bmatrix}$$

Proving that the matrix A is negative-definite is now straightforward by inspecting the sign of the leading principal minors:

$$\begin{cases} A_1 = \partial_\rho \left(\rho^2 \partial_\rho s_{Euler}\right) \leq 0 \\ A_2 = \partial_\rho \left(\rho^2 \partial_\rho s_{Euler}\right) \partial_{e,e} s_{Euler} - \left(\partial_{\rho,e} s_{Euler}\right)^2 \geq 0 \\ A_3 = \rho^{-1} \partial_{\epsilon,\epsilon} s_{rad} A_2 \leq 0 \end{cases} \tag{42}$$

This is easily achieved when assuming that the functions s_{Euler} and s_{rad} are concave. Thus, the sign of (b) is now determined.

Finally, it remains to determine the sign of the term $(c) = \partial_e s \rho \mu (\partial_x u)^2$. The density ρ and the viscosity coefficient μ are both positive: the latest proof for positivity of the density can be found in [19]. Then, only the sign of $\partial_e s$ remains unknown but it can be determined by studying (a). It was assumed earlier in this appendix that $P\partial_e s + \rho^2 \partial_\rho s + \frac{4}{3}\rho\epsilon\partial_\epsilon s = 0$. This equation is now recast and split into two equations using Eq. (41). Separation of variables yields:

$$P\partial_e s_{Euler} + \rho^2 \partial_\rho s_{Euler} = \alpha \text{ and } s_{rad} - \frac{4\epsilon}{3}\partial_\epsilon s_{rad} = \alpha$$

where α is a constant to determine. If one sets $\alpha = 0$, then the two physics are decoupled, which allows us to reconnect to the result derived in [19] for the multi-D Euler equations: $P\partial_e s_{Euler} + \rho^2 \partial_\rho s_{Euler} = 0$. Then, following [19], definitions for $\partial_e s_{Euler}$ and $\partial_\rho s_{Euler}$ are obtained:

$$\begin{cases} \partial_e s = \partial_e s_{Euler} = T^{-1} \\ \partial_\rho s_{Euler} = -\frac{P}{\rho^2} \partial_e s_{Euler} \end{cases}$$

where T is the material temperature which ensures positivity of $\partial_e s$. Thus, (c) is positive.

From the above results, the entropy minimum principle follows, so that the sign of the entropy residual is known:

$$\boxed{\partial_t s + u \partial_x s \geq 0} \tag{43}$$

Remark A.1. *By assuming $\alpha = 0$, an expression for the s_{rad} can be derived by solving the ODE, $s_{rad} - \frac{4\epsilon}{3}\partial_\epsilon s_{rad} = 0$, which yields: $s_{rad}(\epsilon) = \rho^{(0)}\epsilon^{\frac{3}{4}}$, where $\rho^{(0)}$ is a constant. The sign of $\rho^{(0)}$ is determined by using the condition, $\partial_{\epsilon,\epsilon} s_{rad} \leq 0$, derived above, so that $\rho^{(0)} \geq 0$.*

Remark A.2. *The viscous regularization derived in this appendix, has two viscosity coefficients: μ and κ. For the purpose of this paper, these coefficients are set equal. Under this assumption, the above viscous regularization is equivalent to the parabolic regularization of [14].*

References

[1] H. MY, van Leer B, V. R. J, Upwind and high-resolution schemes, Berlin: Springer 12 (1) (1997) 1.

[2] J.-L. Guermond, R. Pasquetti, B. Popov, Entropy viscosity method for nonlinear conservation laws, Journal Comput. Phys. 230 (2011) 4248–4267.

[3] J.-L. Guermond, R. Pasquetti, Entropy viscosity method for high-order approximations of conservation laws, Lecture Notes in Computational Science and Engineering 76 (2011) 411–418.

[4] L. R. J., Numerical methods for conservation laws, Basel: Birhauser, Reading, Massachusetts, 1990.

[5] D. S. Balsara, An analysis of the hyperbolic nature of the equations of radiation hydrodynamics, J. Quant. Spectrosc. Radiat. Transfer 61 (1999) 617–627.

[6] D. W., W. P. R., Numerical simulations for radiation hydrodynamics. i. diffusion limit, Journal of Comput Phys 142 (1998) 182–207.

[7] J. D. Edwards, J. E. Morel, R. B. Lowrie, Second-order discretization in space and time for radiation hydrodynamics, in: International Conference on Mathematics and Computational Methods Applied to Nuclear Science & Engineering (M&C 2013), Sun Valley, Idaho, USA, 2013.

[8] E. Toro, Riemann Solvers and numerical methods for fluid dynamics, 2^{nd} Edition, Springer, 1999.

[9] V. Zingan, J.-L. Guermond, J. Morel, B. Popov, Implementation of the entropy viscosity method with the discontinuous galerkin method, Journal of Comput Phys 253 (2013) 479–490.

[10] R. Lowrie, J. Morel, Issues with high-resolution godunov methods for radiation hydrodynamics, Journal of Quantitative Spectroscopy & Radiative Transfer 69 (2001) 475–489.

[11] R. B. Lowrie, J. D. Edwards, Radiative shock solutions with grey non equilibrium diffusion, Journal of Comput Phys 18 (2008) 129–143.

[12] E. Tadmor, A minimum entropy principle in the gas dynamics equations, Appl. Numer. Math. 2 (1986) 211–219.

[13] P. Lax, Weak solutions of nonlinear hyperbolic equations and their numerical computation, Comm. Pure Appl. Math. 7 (1954) 159–193.

[14] P. B., S. C-W., On positivity preserving finite volume schemes for euler equations, Numer. Math. 73 (1996) 119–130.

[15] S. Jin, C. D. Levermore, Numerical schemes for hyperbolic conservation laws with stiff relaxation terms, Journal of Computational Physics 126 (1996) 449–467.

[16] D. Gaston, C. Newsman, G. Hansen, D. Lebrun-Grandie, A parallel computational framework for coupled systems of nonlinear equations, Nucl. Eng. Design 239 (2009) 1768–1778.

[17] K. D. A., K. D. E., Jacobian-free newton-krylov methods: a survey of approaches and applications, Journal of Computational Physics 193 (2004) 357–397.

[18] R. Berry, R. Saurel, O. LeMetayer, The discrete equation method (dem) for fully compressible, two-phase flows in ducts of spatially varying cross-section, Nuclear Engineering and Design 240 (2010) 3797–3818.

[19] J.-L. Guermond, B. Popov, Viscous regularization of the euler equations and entropy principles, under review.

[20] E. Godlewski, P.-A. Raviart, Numerical approximations of hyperbolic systems of conservation laws, Springer, New-York, 1996.